

Clumped isotope evidence for Early Jurassic extreme polar warmth and high climate sensitivity

Thomas Letulle¹, Guillaume Suan¹, Mathieu Daëron², Mikhail Rogov³, Christophe Lécuyer¹,
Arnaud Vinçon-Laugier¹, Bruno Reynard¹, Gilles Montagnac¹, Oleg Lutikov³, Jan Schlögl⁴.

¹ Univ Lyon, UCBL, ENSL, UJM, CNRS, LGL-TPE, F-69622, Villeurbanne, France

²Laboratoire des Sciences du Climat et de l'Environnement, LSCE/IPSL, CEA-CNRS-UVSQ, Université Paris-Saclay, Orme des Merisiers, F-91191 Gif-sur-Yvette Cedex, France

³Geological Institute of Russian Academy of Sciences, Laboratory of Phanerozoic Stratigraphy.

⁴Comenius University, Faculty of Natural Sciences, Department of Geology and Palaeontology, Mlynská dolina
G, 842 15 Bratislava, Slovak Republik

Correspondence to: Thomas Letulle (thomas.letulle@univ-lyon1.fr)

Abstract. Periods of high atmospheric CO₂ levels during the Cretaceous-Early Paleogene (~140 to ~~33-34~~ My ago) were marked by very high polar temperatures and reduced latitudinal gradients relative to the Holocene. These features represent a challenge for most climate models, implying either higher-than-predicted climate sensitivity to atmospheric CO₂, or systematic biases or misinterpretations in proxy data. Here, we present a reconstruction of marine temperatures at polar (>80°) and mid (~40°) paleolatitudes during the Early Jurassic (~180 My ago) based on the clumped isotope (Δ_{47}) and oxygen-isotope ($\delta^{18}\text{O}_c$) analyses of ~~mildly-shallow~~ buried pristine mollusc shells. Reconstructed calcification temperatures range from ~8 to ~18°C in the Toarcian Arctic and from ~24 to ~28°C in Pliensbachian mid-paleolatitudes. These polar temperatures were ~10-20°C higher than present along with reduced latitudinal gradients. Reconstructed seawater oxygen isotope values ($\delta^{18}\text{O}_w$) of –1.5 to 0.5‰ VSMOW and of –5 to –2.5‰ VSMOW at mid and polar paleolatitudes, respectively, point to a significant freshwater contribution in Arctic regions. ~~This-These data~~ highlight the risk of assuming the same $\delta^{18}\text{O}_{sw}$ value for $\delta^{18}\text{O}$ -derived temperature from different oceanic regions. These findings provide critical new constraints for model simulations of Jurassic temperatures and $\delta^{18}\text{O}_{sw}$ values and suggest that high climate sensitivity is a hallmark of greenhouse climates since at least 180 My.

1 Introduction

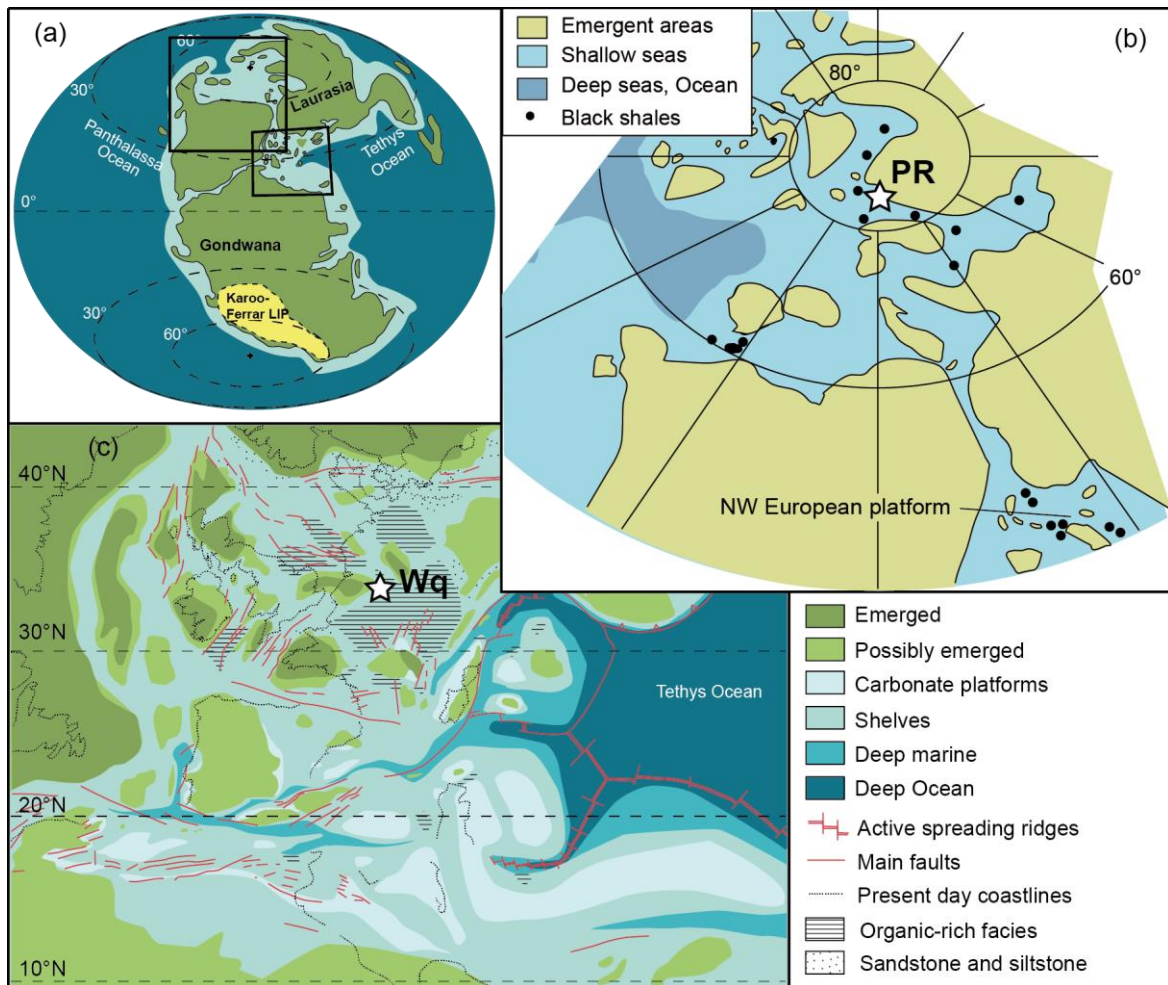
Proxy data indicate that the Cretaceous-Early Paleogene (~140 to ~~33-34~~ My ago) was characterized by high atmospheric CO₂ concentrations, extreme polar warmth and reduced latitudinal temperature gradients (Sluijs et al., 2006; Suan et al., 2017; Evans et al., 2018). Most state-of-the-art climate models hardly reproduce such features, implying either a higher climate sensitivity under greenhouse conditions or systematic biases in proxy data interpretation (Huber and Caballero, 2011; [Laugié et al., 2020](#); Zhu et al., 2020; ~~Laugié et al., 2020~~). It remains unclear whether higher climate sensitivity is unique to the Cretaceous-Early Paleogene world or is rather a hallmark of Earth's climate under high atmospheric pCO₂. Temperature proxies sensitive to ~~overwriting under important~~ burial, such as molecular or clumped-isotope thermometry (Henkes et al., 2014; Fernandez et al., 2021; Hemingway and Henkes, 2021), have seldom been applied to older sediments owing to their generally

40 higher thermal maturity (Robinson et al., 2017; Ruebsam et al., 2020; Fernandez et al., 2021). Consequently,
current temperature estimates ~~for ante-predating the~~ Cretaceous periods are mostly derived from the oxygen
isotope composition of marine carbonate fossils ($\delta^{18}\text{O}_c$), with well-known limitation related to uncertainties in
the past $\delta^{18}\text{O}$ signature of seawater ($\delta^{18}\text{O}_w$) (Epstein et al., 1953; Roche et al., 2006; Laugié et al., 2020).
Here, we use carbonate clumped isotope thermometry (Δ_{47}), to simultaneously constrain the calcification
45 temperatures and associated $\delta^{18}\text{O}_w$ values of marine carbonate shells (mostly aragonite) collected from Lower
Jurassic sedimentary successions with exceptionally shallow to moderate burial depths spanning subtropical to
polar paleolatitudes. We compare our results to existing Jurassic to Eocene climate proxy data and simulations
and discuss their implications for climate sensitivity under greenhouse conditions.

50 2 Geological settings

2.1 Polovinnaya River

The Polovinnaya River section is located in northern Siberia (72°36'05" N, 107°58'52.2" E), and was located
near the north pole during the early-Early Jurassic (Fig. 1). Our bivalve samples come from between 0 and 14m
in the section and belong to the Toarcian (Suan et al., 2011). This interval consists of silty shale slightly enriched
55 in organic carbon (TOC ~0.5%). Except for localized carbonate concretions, there is no carbonate fraction in the
sediment. The studied interval has been previously correlated to the lower Toarcian Serpentinum ammonite zone
based on biostratigraphy of foraminifera and dinoflagellate cyst, and lithostratigraphic correlation with other
sections of the basin (Suan et al., 2011). This section records very abundant *Dacryomya* bivalve shells (Fig. S1),
an opportunistic suspension-feeder genus tolerant to poorly oxygenated waters, which preferred conditions with
60 weak hydrodynamics (Zakharov and Shurygin, 1978). Few belemnite rostra were also recorded as well as
isolated fish scales and teeth. Overall the fossil assemblage indicates fully marine conditions within proximity of
the continents as evidenced by the occurrence of wood debris. The section has undergone ~~exceptionally~~-low
burial as suggested by the low values of Rock-Eval Pyrolysis T_{max} (mean = 420°C) previously measured in the
host sediments (Suan et al., 2011). Regional stratigraphy from the more distal Anabar area suggests local
65 overburden not exceeding 1000_m: a total overburden (Lower Toarcian to Valanginian) of about 380_m is
recorded in the Anabar River area (Nikitenko et al., 2013) located 200 km East of the Polovinnaya section,
which may be extended to about 1000_m when adding Valanginian-Cenomanian overburden from the more distal
Bol'shoi Begichev islands. Modern local geothermal fluxes are lower than 50 mW/m^2 (Kerimov et al., 2020),
indicative of a low geothermal gradient (<25°C/km). Assuming a warm mean surface temperature of 10°C, the
70 1000 m of overburden and assuming that the geothermal gradient of the Siberian craton did not significantly
change in the last 200 My, maximum burial temperatures of around 35°C can be estimated for the studied
specimens from Polovinnaya river.



75 **Figure 1. Location of the studied sites with regard to Toarcian (Early Jurassic) geography.** (a) Global map modified from Dera et al. (2009). (b) Arctic map modified from Nikitenko and Mickey (2004). (c) Tethyan map modified from Thierry, (2000). Localities: PR = Polovinnaya River; Wq = Warcq.

2.2 Warcq

80 Samples from north-eastern Paris Basin were collected in 2014 from a temporary road cutting located near Warcq, Ardennes, France (49°45'21.6"N, 4°39'28.8"E). They consist of grey silty claystone with lenses of packed carbonated shell fragments, mainly from a variety of bivalves (*Grammatodon*, *Malletia*, *Limea*, *Oxytoma*) and few ammonoids (*Beaniceras*, *Aegoceras?*, *Dactylioceratidae*) (Fig. 2). The lithology, fossil preservation and assemblages of the sampled beds ~~is~~are similar to those described by Thuy et al. (2011), from a nearby site of Sedan and dated from the Pliensbachian Davoei zone. The sampled levels are therefore tentatively attributed to the lower Pliensbachian Davoei ammonite zone. Mean T_{\max} values of 425°C and maximum burial temperatures near 60°C have been reported for Pliensbachian sediments from NE Paris Basin boreholes where the Davoei zone bears at ~1100 m deep in the EST 433 borehole, some 150 km south from Warcq (Blaise et al., 2014), and lies at ~860 m in the Montcornet borehole, some 50 km west from Warcq (Disnar et al., 1996; Bougeault et al., 2017), of the NE Paris Basin (Disnar et al., 1996; Blaise et al., 2014). These burial temperatures and depths should be regarded as an upper limit, as the very proximal sampling area near Warcq was repeatedly emerged during the Mesozoic and hence shows a much-thinner Mesozoic cover of ~500 m than these more distal sites (Waterlot et al., 1960). Assuming 860 m of overburden, ~300m of Cretaceous overburden eroded during the

85

90

Cenozoic based on Paris basin thermal history (Brigaud et al., 2020), a Mesozoic surface temperature of ~20 °C and canonical continental geothermal gradient of ~35 °C/km, maximal burial temperature of ~60 °C can be estimated for the studied specimens from Warcq.



100 **Figure 2. Selected specimens from the sampled successions.** (a-d). Polovinnaya River section (Toarcian), (e-l). Warcq section (Pliensbachian); (a). *Dacryomya jacutica*, specimen Pol 29 (on the surface of a carbonate concretion); (b). *Dacryomya jacutica*, specimen Pol 13; (c-d). *Dacryomya jacutica*, specimen Pol 5; (e-f). *Grammatodon* sp., specimen ARD-01 (inner mould after sampling of the shell); (g-h). *Malletia* sp.; (i).

105 *Limea* sp., specimen ARD-03 (inner mould after sampling of the shell); (j). *Oxytoma* sp.ind. (inner mould with remains of a calcite shell) (k). *Aegoceras?*, specimen ARD 06; (l). Dactylioceratidae indet., specimen ARD-07.

3 Material and Methods

3.1 Sampled material

110 The two studied sites present exceptionally rare records of aragonite preservation for the Lower Jurassic interval. *Dacryomya* shells are the most abundant macrofossil and the unique bivalve genera only bivalve genus to occur in the Polovinnaya River section. They are very abundant in the lower part of the section (0 to 8 m). They are mainly represented by adult shells, while juveniles are common in only few levels. They appear as ~1 cm distinct individual or detached valves, sometimes close to each other (Fig. 2). The carbonate shells, ~~often~~ commonly flattened and partially to entirely preserved, are a few millimetres thick but brittle and detached easily from their inner and outer mould. Their cream to white colour contrasts with the dark aspect of the sediment, and few thicker individuals are iridescent.

Molluscs shells from Warcq, clearly show a more energetic environment as they mostly appear as packed shell fragments showing a higher taxonomic diversity relative to the other site. Few complete individuals and separated valves can be observed among the debris with their associated mould in or around the remaining shell. Shells are cream to clear white, with some showing iridescence.

The remnants of carbonate shells were sampled as a whole using dental tools under a binocular-microscope. A carbonate vein and the matrix from the carbonate nodule Pol 29 were also sampled to constrain the geochemistry of this potential diagenetic phase.

125 The microstructural preservation state and mineralogy of the analysed bivalve and ammonite shells were investigated using a Phenom Pure G2 scanning electron microscope (SEM) in backscatter mode (~~BSEM-G2~~) and Raman spectroscopy using an XploRA Raman microscope in Laboratoire de Géologie de Lyon (LGLTPE). SEM observations were performed on relatively large fragments (few millimetres wide) of the most complete specimens. Raman spectra were acquired either directly on the fossil specimens partly enclosed in the sedimentary matrix, or on several grains of the sampled powders.

3.2 Geochemical analysis and data processing

135 ~~The remnants of carbonate shells were sampled as a whole using dental tools under a binocular microscope. A carbonate vein and matrix from the carbonate nodule Pol 29 were also sampled to constrain the geochemistry of this potential diagenetic phase.~~

140 The Δ_{47} and $\delta^{18}\text{O}$ values of ~~153~~ samples were measured (1 to 5 replicates each) using methods described by (Daëron et al., (2016). Carbonate samples were converted to CO_2 by phosphoric acid reaction at 90-°C in a common, stirred acid bath for 15 minutes. Initial phosphoric acid concentration was 103 % (1.91 g/cm³) and each batch of acid was used for 7 days. After cryogenic removal of water, the evolved CO_2 was helium-flushed at 25 mL/min through a purification column packed with Porapak Q (50/80 mesh, 1 m length, 2.1 mm ID) and held at -20-°C, then quantitatively recollected by cryogenic trapping and transferred into an Isoprime 100 dual-

145 inlet mass spectrometer equipped with six Faraday collectors (m/z 44–49). Each analysis took about 2.5 hours,
during which analyte gas and working reference gas were allowed to flow from matching, 10 mL reservoirs into
the source through deactivated fused silica capillaries (65 cm length, 110 μm ID). Every 20 minutes, gas
pressures were adjusted to achieve $m/z = 44$ current of 80 nA, with differences between analyte gas and working
gas generally below 0.1 nA. Pressure-dependent background current corrections were measured 12 times for
each analysis. All background measurements from a given session are then used to determine a mass-specific
150 relationship linking background intensity (Z_m), total $m/z = 44$ intensity (I_{44}), and time (t): $Z_m = a + bI_{44} + ct +$
 dt^2 . Background-corrected ion current ratios (δ_{45} to δ_{49}) were converted to $\delta^{13}\text{C}$, $\delta^{18}\text{O}$, and “raw” Δ_{47} values as
described by Daëron et al., (2016), using the IUPAC oxygen-17 correction parameters. The isotopic composition
($\delta^{13}\text{C}$, $\delta^{18}\text{O}$) of our working reference gas was computed based on the nominal isotopic composition of carbonate
standard ETH-3 (Bernasconi et al., 2018) and an oxygen-18 acid fractionation factor of 1.00813 (Kim et al.,
155 2007). Raw Δ_{47} values were then converted to the I-CDES Δ_{47} reference frame by comparison with four “ETH”
carbonate standards (Bernasconi et al., 2021) using a pooled regression approach (Daëron, 2021). Full analytical
errors are derived from the external reproducibility of unknowns and standards ($N_f = 89$) and conservatively
account for the uncertainties in raw Δ_{47} measurements as well as those associated with the conversion to the
“absolute” Δ_{47} reference frame.

160 Complementary $\delta^{13}\text{C}$ and $\delta^{18}\text{O}$ analyses of the smallest Arctic shells were performed at LGLTPE, using a
MultiprepTM automated sampler coupled to a dual-inlet GV IsoprimeTM mass spectrometer. Samples were
reacted with anhydrous phosphoric acid at 90°C. Duplicated samples were adjusted to the international
references NIST NBS 18 and NBS 19 as well as in-house standard Carrara Marble. Since 2019 overall
reproducibility of the in-house standard Carrara Marble are $\pm 0.082\text{--}0.088$ for $\delta^{18}\text{O}$ (2 SE, $n = 441\text{--}649$) and ± 0.057
165 064 ‰ for $\delta^{13}\text{C}$ (2 SE, $n = 441\text{--}649$) with mean $\delta^{18}\text{O}$ and $\delta^{13}\text{C}$ values, respectively of - 1.041 ‰ and +2.025 ‰
(V-PDB). All carbonate isotopic values ($\delta^{13}\text{C}$, $\delta^{18}\text{O}_c$) are reported in ‰ VPDB.

Clumped isotope temperatures were computed based on the I-CDES calibration of (Anderson et al., 2021).
Temperature uncertainties correspond to the fully-propagated 95% confidence intervals from Δ_{47} measurements
of each sample (Daëron, 2021), neglecting the much smaller uncertainties in the calibration. The $\delta^{18}\text{O}$ values
170 from aragonite samples were adjusted considering the different phosphoric acid fractionation factors for calcite
and aragonite (Kim et al., 2007). The $\delta^{18}\text{O}_w$ values relative to VSMOW was estimated using Δ_{47} -derived
temperatures and the equations of Grossman and Ku (1986) and Kim and O’Neil (1997) for mollusc shells and
calcite vein respectively.

Paleolatitude of the studied sites was computed using the online paleolatitude calculator paleolatitude.org (van
175 Hinsbergen et al., 2015) computed with the model of Torsvik et al. (2012).

4 Results

180 ~~The SEM observations of shell fragments of *Daeryomya jacutica* revealed well-preserved sheet nacreous
microstructures underlying a prismatic layer we interpret as the outer shell layer (Fig. 3). All Raman spectra
gathered from *Daeryomya jacutica* shells confirm that the original aragonite mineralogy is preserved. Mollusk
shells from Wareq showing an aragonite mineralogy revealed microstructures similar to those observed in
Daeryomya jacutica, the main differences being that sheet nacreous structures of the studied ammonite shell~~

(ARD-05) shows thinner tablets than those of bivalve shells (Fig. 3). Both SEM and Raman data indicate that the sample ARD-03 (bivalve fragment) is in calcite, showing a darker colour and no iridescence, with a much simpler and massive structure observed in SEM (Fig. 3).

Reconstructed Δ_{47} temperatures range from $8.5 \pm 5.2^\circ\text{C}$ to $17.7 \pm 3.4^\circ\text{C}$ for Siberian bivalves, from $24.1 \pm 4.38^\circ\text{C}$ to $27.6 \pm 3.3^\circ\text{C}$ for molluscs from NE France, while for the fracture infilling calcite vein from Siberia a temperature of $31.1 \pm 4.8^\circ\text{C}$ is inferred. Mean $\delta^{18}\text{O}_e$ values are $-2.73 \pm 0.71\text{‰}$ (1SD, n=31, Max=0.36, Min=-5.08‰) for Siberian bivalves and $-14.21 \pm 0.02\text{‰}$ for the fracture infilling calcite vein, and $-2.07 \pm 0.86\text{‰}$ (1SD, n=4, Max= -0.84‰, Min= -2.54‰) for molluscs from NE France. The carbon isotope values ($\delta^{13}\text{C}$) range from 0.37‰ to 2.82‰ in the selected molluscs from Wareq, from 3.47‰ to 5.09‰ in the Russian Arctic bivalves, and reach values down to -21.43‰ and -4.67‰ for carbonate nodule matrix and the embedded bivalve shells (sample POL-29) respectively.

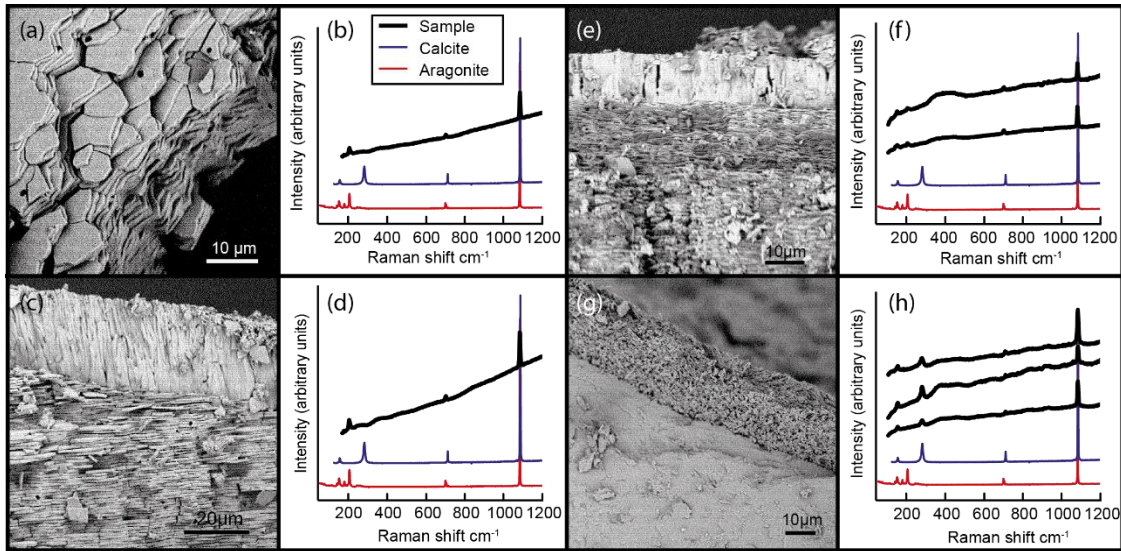
The calculated $\delta^{18}\text{O}_w$ values range from $0.5 \pm 0.7\text{‰}$ to $-1.5 \pm 1.0\text{‰}$ in molluscs from NE France, from $-4.88 \pm 1.20\text{‰}$ to $-2.52 \pm 0.78\text{‰}$ in Siberian bivalves. A much lower value of $-10.6 \pm 0.9\text{‰}$ is obtained for the fracture infilling calcite vein from Polovinnaya River.

4.1 Polovinnaya River, Siberia

The SEM observations of shell fragments of *Dacryomya jacutica* revealed well-preserved sheet nacreous microstructures underlying a prismatic layer we interpret as the outer shell layer (Fig. 3). All Raman spectra gathered from *Dacryomya jacutica* shells confirm that the original aragonite mineralogy is preserved.

Δ_{47} range from 0.6151 ± 0.0108 to $0.6457 \pm 0.0182\text{‰}$ I-CDES for Siberian aragonite bivalves, and a Δ_{47} of 0.5752 ± 0.0134 for the fracture-infilling calcite vein. Reconstructed Δ_{47} temperatures, applying the equation of Anderson et al., (2021), range from $8.8 \pm 5.2^\circ\text{C}$ to $18.0 \pm 3.4^\circ\text{C}$ for Siberian bivalves, and $31.5 \pm 4.8^\circ\text{C}$ for the calcite vein.

Mean $\delta^{18}\text{O}_e$ values are $-2.73 \pm 0.71\text{‰}$ (1SD, n=31, Max=0.36, Min=-5.08‰) for Siberian bivalves and $-14.21 \pm 0.02\text{‰}$ for the fracture-infilling calcite vein while the carbon isotope values ($\delta^{13}\text{C}$) range, from 3.47‰ to 5.09‰ in bivalve shells, and reach values down to -21.43‰ and -4.67‰ for carbonate nodule matrix and the embedded bivalve shells (sample POL-29) respectively. Using the Δ_{47} -derived temperature to estimate the oxygen isotope fractionation factor results in $\delta^{18}\text{O}_w$ values ranging from $-4.88 \pm 1.20\text{‰}$ to $-2.52 \pm 0.78\text{‰}$ in Siberian bivalves. A much lower value of $-10.6 \pm 0.9\text{‰}$ is obtained for the fracture-infilling calcite vein from Polovinnaya River.

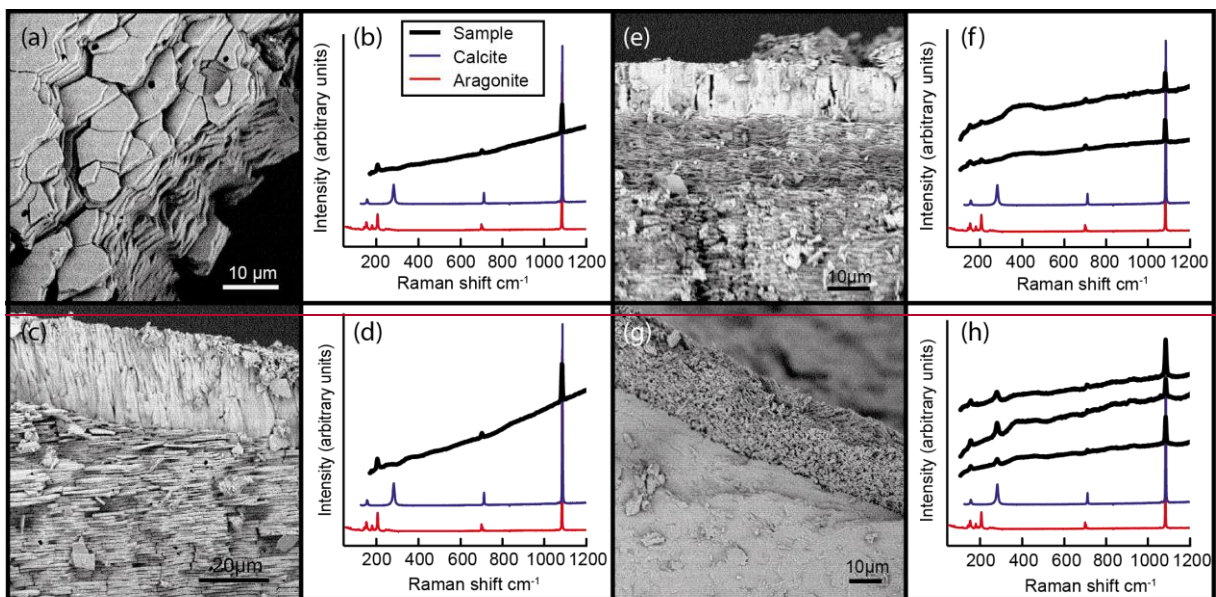


215 **Figure 3. SEM images and Raman spectra for a selection of samples.** a, c, e and g SEM images from of
 samples POL-8, POL-12, ARD-05 and ARD-03 respectively. b, d, f and g Raman spectra from of samples POL-
 8, POL-12, ARD-05 and ARD-03 compared to the reference spectra of calcite and aragonite.

4.2 Warcq, France

220 Mollusc shells from Warcq showing an aragonite mineralogy revealed microstructures similar to those observed
 in *Dacryomya jacutica* from Siberia, the main differences being that sheet nacreous structures of the studied
 ammonite shell (ARD-05) shows thinner tablets than those of bivalve shells (Fig. 3). Both SEM and Raman data
 indicate that the sample ARD-03 (bivalve fragment) is in calcite, showing a darker colour and no iridescence,
 with a much simpler and massive structure observed in SEM (Fig. 3).

225 Δ_{47} of measured bivalve and ammonite shells from Warcq range from 0.5851 ± 0.0095 to 0.5955 ± 0.0130 ‰ I-
 CDES. Reconstructed Δ_{47} temperatures range from $24.4 \pm 4.4^\circ\text{C}$ to $28.0 \pm 3.3^\circ\text{C}$. Mean $\delta^{18}\text{O}_c$ values are
 -2.30 ± 0.76 ‰ (1SD, n=6, Max=-0.83‰, Min=-2.79‰), and $\delta^{13}\text{C}$ range from 0.37‰ to 2.82‰. The calculated
 $\delta^{18}\text{O}_w$ values range from 0.6 ± 0.7 ‰ to -1.4 ± 1.0 ‰.



230

235

~~Figure 3. SEM images and Raman spectra for a selection of samples. a, c, e and g SEM images from samples POL-8, POL-12, ARD-05 and ARD-03 respectively. b, d, f and g Raman spectra from samples POL-8, POL-12, ARD-05 and ARD-03 compared to the reference spectra of calcite and aragonite.~~

5 Discussion

240

5.1 Sample preservation

245

The SEM and Raman observations reveal that the analysed mollusc shells from both sites retain pristine aragonite mineralogy and microstructures with ~~no~~ neither evidence of recrystallization nor mineralogical conversion (Fig. 3). Despite their aragonite mineralogy, the *Dacryomya* shells from sample Pol-29 record unusually low $\delta^{13}\text{C}$ that are $\sim 8\%$ lower than the other *Dacryomya* shells analysed from the same succession. The carbonate matrix of the nodule where these shells are embedded also records a very low $\delta^{13}\text{C}$ value (-21.43%) but a $\delta^{18}\text{O}$ value within the range of the bivalve shells. We therefore attribute the extremely low $\delta^{13}\text{C}$ values of bivalve shells of this level to an early diagenetic phase resulting in the formation of carbonate nodules derived from respiratory CO_2 that locally altered the bivalve shells geochemistry.

250

Organic matter maturity, mineralogical and sedimentological data all imply exceptionally shallow burial depth (< 1 km) for the samples investigated here. Maximum burial temperature (T_{burial}) remained well below the commonly assumed minimum temperature ($80\text{--}120^\circ\text{C}$) of solid-state reordering of C-O bonds in calcite at such geological timescales (Henkes et al., 2014; Stolper and Eiler, 2015; Hemingway and Henkes, 2021). Recent experiments show that aragonite is more susceptible to solid-state bond reordering (Chen et al., 2019), but there is to our knowledge no existing model constraining the temperatures at which this process would markedly

255

overwrite the Δ_{47} value of this mineral at such time scales. The exceptional preservation of aragonite nacreous sheet microstructures in these samples implies minimal amounts of fluid circulation and recrystallization, if any. Exchange between fluid inclusions in mollusc shells and the surrounding carbonate minerals was recently suggested as an alternative process that may alter the clumped isotope signature of biogenic carbonates without substantially affecting the stable isotope signature of the shell nor its mineralogy (Nooitgedacht et al., 2021). In their heating experiments, these exchanges resulted in a significant decrease of the Δ_{47} value of the bivalve shells compared to the original shell, and a minor ($\sim 0.1\%$) decrease in $\delta^{18}\text{O}$ of the heated shell. We cannot exclude that this process has altered the fossils studied here even at low temperature, nor do we have evidence that it occurred. The Δ_{47} temperature of $31.1 \pm 4.8^\circ\text{C}$ for the fracture-infilling calcite vein in Arctic Russia is significantly higher than those inferred from bivalves and is consistent with a formation depth < 1 km assuming a geothermal gradient of $25^\circ\text{C}/\text{km}$. The reconstructed $\delta^{18}\text{O}_w$ value of $-10.7 \pm 0.9\%$ for this calcite vein is also substantially lower than those inferred from associated bivalves, consistent with a late-phase meteoric source for the mineralizing fluid. The precise depth and date at which this vein formed however, remain uncertain.

260

265

270 Based on the geological setting of the samples and their preservation, we consider any substantial alteration of
their original geochemical signature unlikely. In the remote scenario that the studied material has been slightly
modified by solid-state bond reordering, one would expect the Δ_{47} of the samples to be lower than their original
values (Henkes et al., 2014; Stolper and Eiler, 2015; Fernandez et al., 2021; Hemingway and Henkes, 2021).
Therefore, both the temperature and $\delta^{18}\text{O}_w$ reported here would be overestimated, and should be taken as an
275 upper limit of original environmental parameters.

5.2 Evidence for extreme warmth and reduced salinity in the Arctic during the Toarcian Oceanic Anoxic Event

280 Bivalve shells record a marked rise in $\delta^{13}\text{C}$ along the section up to $\sim 5\%$ that parallels that recorded by organic carbon $\delta^{13}\text{C}$ data (Fig. 4; Suan et al., 2011). These results strengthen the correlation of the corresponding part of the succession with the rising limb of the positive carbon isotope excursion commonly used to characterise the termination of T-OAE interval in coeval sites of Europe and North Africa (Jenkyns and Clayton, 1986; Suan et al., 2010; Krencker et al., 2014; Baghli et al., 2020; Ullmann et al., 2020; Baghli et al., 2020). Bivalve shells
285 $\delta^{18}\text{O}_c$, however, show no stratigraphic trend as opposed to brachiopod shell T-OAE records from western Tethys at mid-latitudes (Suan et al., 2010; Krencker et al., 2014; Ullmann et al., 2020; Baghli et al., 2020). Our Δ_{47} results yield polar temperatures ranging from 8.5 ± 5.2 to 17.7 ± 3.4 °C (Mean=14.7°C, n=8). As it occurs with most Δ_{47} -derived temperature datasets, the relatively large uncertainties of the present estimates of Siberian SST hamper the identification of distinctive stratigraphic trends.

290 Bivalve shell growth can be highly variable during the animal life (Schöne, 2008), making any paleoenvironmental record derived from bivalve shell either incomplete (because of growth cessation) or at least biased towards the period of maximum growth rate. Shell growth rate can be controlled by both environmental parameters (Temperature, salinity, food availability, ...)—biological processes such as spawning, and changes during the ontogeny (Schöne, 2008). One major aspect of shell growth that may bias the geochemical signal data
295 is seasonal shell growth-cessation. In modern high-latitude bivalves, seasonal shell growth-cessation generally occurs during the winter, triggered by low temperatures or low food availability (Peck et al., 2000; Vihtakari et al., 2016; Killam and Clapham, 2018). ~~It appears likely that food availability declined markedly during the Early Jurassic polar night, which would have certainly led to winter growth cessation in the analysed *Dacryomya* shells.~~ In the present-day *Nucula annulata*, an aragonite bivalve with similar ecology to the analysed *Dacryomya*
300 *jacutica*, growth cessation occurs in winter and during spawning at peak local temperatures, its average $\delta^{18}\text{O}_c$ hence records late spring to early fall SST (Craig, 1994). By contrast, growth band $\delta^{18}\text{O}_c$ offers evidence for summertime-only growth cessation in high-latitude Eocene bivalves from Antarctica, with inferred winter SST of 11.1 ± 0.6 and summer SST of 17.6 ± 1.3 °C (Buick and Ivany, 2004; Douglas et al., 2014) ~~very close to our maximal and minimum SST estimates of the Toarcian Arctic.~~ A comparable seasonal $\delta^{18}\text{O}_c$ record could not be
305 generated from our Russian Arctic material owing to the very small size of the available *Dacryomya* shells (1 to 2cm). In any case, the temperate data from NE France should be minimally affected by seasonal biases as shell precipitation occurs more continuously throughout the year in modern temperate molluscs (Killam and Clapham, 2018). Besides, both sites were deposited in ~~near-near~~-shore environments at very shallow depths likely not

310 exceeding a few tens of meters (Suan et al., 2011; Thuy et al., 2011; Suan et al., 2014). Although bivalves from both sections record temperatures near the sea bottom that were likely slightly cooler than the sea surface, the difference should not have exceeded a few degrees, owing to their shallow living depth we expect the studied bivalves to have lived within the thermocline. We therefore conservatively interpret the reconstructed temperatures as reflecting polar warm-season SST (summer; SST_{PWS}) in Arctic Russia and low latitude annual SST in NE France. These SST_{PWS} for the T-OAE are still 10-20°C higher than present-day SST_{PWS} (Fig. 5).

315 The reconstructed polar $\delta^{18}\text{O}_w$ values ranging from -4.9 ± 1.2 to $-2.5 \pm 0.8\text{‰}$ VSMOW during the T-OAE are significantly lower than the value of -1‰ VSMOW expected for an ice-free world mean open ocean (Shackleton and Kennett, 1975). These results imply a substantial freshwater contribution to the studied basin during the T-OAE, probably resulting from coastal runoff at this relatively proximal site, ~~as evidenced from abundant terrestrial organic matter~~ (Suan et al., 2011). High temperatures and reduced salinity are in broad agreement with

320 paleontological evidence for warm and humid temperate conditions during the T-OAE interval in Arctic Siberia (Rogov et al., 2019). Brackish conditions are also consistent with the fossil assemblages of the succession that includes abundant terrestrial organic matter and wood debris, marine to brackish elements such as abundant dinoflagellate cysts, benthic foraminifera (preserved as organic linings and agglutinate forms) and typically marine elements that are represented by a few belemnite rostra and unidentifiable ammonite internal moulds (Suan et al., 2011). Interestingly, protobranch bivalves, to which *Dacryomya* belongs, are not well adapted to

325 salinities lower than 20‰ (Zardus, 2002). Assuming a similar lower salinity limit for Polovinnaya River bivalves, a global mean ocean with a salinity of 34.5‰ and a $\delta^{18}\text{O}_w$ of -1‰ VSMOW, mass balance considerations (see Supplementary Data) imply an upper limit of $\sim -8\text{‰}$ VSMOW for local $\delta^{18}\text{O}$ of precipitations and runoff ($\delta^{18}\text{O}_p$). This value is high relative to modern Arctic $\delta^{18}\text{O}_p$ but in agreement with the prediction that higher polar temperatures should have produced higher $\delta^{18}\text{O}_p$ than those prevailing today (Rozanski et al., 1992). Similarly, terrestrial plants *n*-alkanes hydrogen isotopes and paleosol siderite Δ_{47} data indicate slightly lower Arctic $\delta^{18}\text{O}_p$ of -10 to -15‰ VSMOW during the Early Eocene Arctic coast salinity can be inferred from Δ_{47} -derived $\delta^{18}\text{O}_w$ with reasonable assumptions of local $\delta^{18}\text{O}$ of precipitations and runoff ($\delta^{18}\text{O}_p$). Higher polar temperatures should have produced higher $\delta^{18}\text{O}_p$ than those prevailing today (Rozanski et al., 1992), a hypothesis supported by terrestrial plants *n*-alkanes hydrogen isotopes and paleosol siderite Δ_{47} data indicating Early Eocene $\delta^{18}\text{O}_p$ of -10 to -15‰ (Pagani et al., 2006; van Dijk et al., 2020), another well-established warm period with evidence of polar warmth (Markwick, 1998; Sluijs et al., 2006, 2020; Douglas et al., 2014; Suan et al., 2017; van Dijk et al., 2020).

330 ~~Assuming a similar range of $\delta^{18}\text{O}_p$ values in the Early Jurassic Arctic, and the assumption listed above for the Early Jurassic oceans, and a global mean ocean with a salinity of 34.5‰ and a $\delta^{18}\text{O}_w$ of -1‰ , mass balance calculations indicate mean salinity of $23.9 \pm 2.9\text{‰}$ (1σ , $n=8$) and $27.7 \pm 1.8\text{‰}$ (1σ , $n=8$) with $\delta^{18}\text{O}_p$ of -10 and -15‰ VSMOW, respectively (see Supplementary Data), again consistent with paleontological evidence suggesting. ~~These estimates point towards~~ brackish waters at Polovinnaya River during the Toarcian, ~~consistent with the fossil assemblages of the succession that includes abundant terrestrial organic matter and wood debris, marine to brackish elements such as abundant dinoflagellate~~~~

335 ~~cysts, benthic foraminifera (preserved as organic linings and agglutinate forms) but rarer typically marine elements that are only represented by a few belemnite rostra and unidentifiable ammonite internal moulds~~ (Suan et al., 2011). Such values are also comparable to the salinity of 28‰ estimated using a fully coupled ocean–atmosphere model for the Toarcian (Dera and Donnadieu, 2012), although the Arctic temperature obtained by

340

345

the same model are in strong disagreement with our data (Fig. 5). Such observations should be replicated around the Arctic realm to test whether the brackish environment evidenced here ~~is~~ was of local or more regional nature.

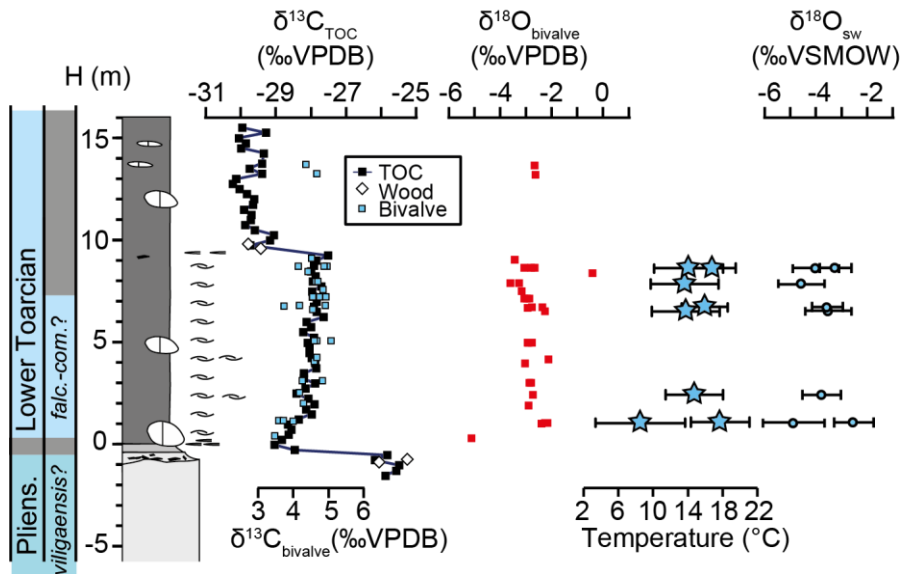


Figure 4. Geochemical record of the T-OAE at Polovinnaya River, Arctic Siberia. Stratigraphy and biostratigraphic zones are for the Arctic realm (falc.=Falciferum zone, com.=Commune zone). The organic carbon isotope ($\delta^{13}\text{C}_{\text{TOC}}$) data (black squares) wood debris $\delta^{13}\text{C}$ data (white diamonds) are from Suan et al. (2011); the bivalve shell $\delta^{13}\text{C}$ data (blue squares), bivalve shell $\delta^{18}\text{O}$ (red squares), Δ_{47} temperatures (blue stars), and $\delta^{18}\text{O}_w$ estimates (blue circles) inferred from bivalve shells Δ_{47} values are from this study. Stratigraphy and organic carbon isotope ($\delta^{13}\text{C}_{\text{TOC}}$) data from Suan et al. (2011). The analysed bivalve samples all belong to the species *Dacryomya jacutica*. Δ_{47} -derived temperatures were computed using the equation of Anderson et al. (2021). $\delta^{18}\text{O}_w$ was calculated using the oxygen isotope fractionation equation of Grossman and Ku (1986).

5.3 Early Jurassic latitudinal temperature and $\delta^{18}\text{O}_w$ gradients

The mid-mid-paleolatitude SST reconstructed by our new clumped isotope data ($\sim 25^\circ\text{C}$) are in good agreement with recent Sinemurian-Pliensbachian and Toarcian $\text{TEX}_{86}^{\text{H}}$ data pointing to summer SST $\sim 20\text{--}30^\circ\text{C}$ at slightly lower paleolatitudes (Robinson et al., 2017; Ruebsam et al., 2020). It should be noted that the mid-latitude samples presented here are from the Davoei Zone and predate the T-OAE interval recorded by the Siberian data by ~ 6 million years. Nevertheless, climate proxies from the Davoei zone indicate the corresponding time interval, although likely slightly cooler than the T-OAE, correspond to one of the warmest period of the Early Jurassic (Dera et al., 2011; Bougeault et al., 2017). The new clumped isotope data from the two sites, even if they are not strictly contemporaneous, can therefore be reasonably used to tentatively estimate latitudinal gradient during the warmest episodes of Early Jurassic. The Δ_{47} data presented herein suggest a decrease in mean SST of $0.26 \pm 0.05^\circ\text{C}$ per $^\circ$ of latitude between mid and high latitudes, i.e., a reduction of the latitudinal SST gradient of $32 \pm 10\%$ relative to present, consistent with the most conservative Early Eocene estimates (Evans et al., 2018). Comparing our Siberian T-OAE Δ_{47} temperatures with contemporaneous $\text{TEX}_{86}^{\text{H}}$ temperatures estimated for low latitudes (Ruebsam et al., 2020) results in an even shallower gradient of $0.17 \pm 0.05^\circ\text{C}$ per $^\circ$ of latitude between low and high latitudes.

Considering the scarcity of other Early Jurassic temperature proxy-data, model-based SST and $\delta^{18}\text{O}_w$ estimates, we extend the comparison to SST and $\delta^{18}\text{O}_w$ estimates based on various proxy-data and published Earth system

simulations for other Jurassic to Eocene intervals (Fig. 5; Supplement). ~~This compilation shows that Δ_{47} -SST from NE France agree with most previous $\text{TEX}_{86}^{\text{H}}$ and Δ_{47} -SST for the Jurassic-Eocene interval, with values $> 5^{\circ}\text{C}$ higher than present-day SST. First, the new Δ_{47} temperatures can be compared with other well established warm intervals, such as the Cenomanian-Turonian and the Eocene. The compilation shows that Δ_{47} -SST from NE France agree with most previous mid-latitude $\text{TEX}_{86}^{\text{H}}$ and Δ_{47} -SST for the Eocene interval ($20\text{-}30^{\circ}\text{C}$), with values $> 5^{\circ}\text{C}$ higher than present-day SST. Mid-latitude Cenomanian-Turonian $\text{TEX}_{86}^{\text{H}}$ SST are significantly higher ($>30^{\circ}\text{C}$) and form the highest mid-latitude temperature of the compilation. High latitude data are much more scarce. Still, Russian Arctic Toarcian SST are very close to Early Eocene polar SST derived from Arctic (Sluijs et al., 2006, 2020; Suan et al., 2010) and Antarctic (Douglas et al., 2014) sites with polar SST $>15^{\circ}\text{C}$ warmer than present during these two distinct greenhouse period (Fig. 5). This comparison also shows that the Maastrichtian was characterized by substantially lower Δ_{47} -SST, in line with independent evidence for global cooling during this interval (O'Brien et al., 2017; Pucéat et al., 2003), although many Δ_{47} records from this stage come from the Western Interior Seaway (WIS) where temperatures were likely influenced by specific regional patterns, such as southward influence of arctic water or significant freshwater contribution in the basin (Coulson et al., 2011; Petersen et al., 2016). This compilation also reveals lower SSTs near 50°N in the Callovo-Oxfordian. Russian Arctic SST are very close to Campanian-Maastrichtian and Early Eocene $\text{TEX}_{86}^{\text{H}}$ -derived SST (Jenkyns et al., 2004; Sluijs et al., 2020) and Early Eocene bioclimatic SST (Suan et al., 2017) from the Arctic (Fig. 5). The Δ_{47} -data presented herein suggest a decrease in mean SST of $0.26\pm 0.05^{\circ}\text{C}$ per $^{\circ}$ of latitude, i.e., a reduction of the latitudinal SST gradient of $32\pm 10\%$ relative to present, consistent with the most conservative Early Eocene estimates (Evans et al., 2018).~~

Our Δ_{47} SST for the Lower-Jurassic can be compared to published results from Earth System models that simulate ~~past these~~ intervals of global warmth (see previous paragraph) to discuss model-data discrepancies, especially apparent at high-latitudes. Proxy-data indicate an atmospheric pCO_2 of 1000 ± 500 ppmv during the Early Jurassic, with maximum values of 1750 ± 500 ppmv, i.e., 6x pre-industrial levels (PIL), during the T-OAE (McElwain et al., 2005; Li et al., 2020). Earth system models run at 6x PIL for Early Jurassic (Dera and Donnadieu, 2012) or Cretaceous-Eocene paleogeography almost invariably produce lower SST than those inferred from our Δ_{47} data, with a maximum model-data discrepancy of $>15^{\circ}\text{C}$ at high latitudes (Fig. 5). To achieve such polar warmth, the Eocene CCSM3 simulations require 16x PIL, more than twice that indicated by Lower Jurassic and Eocene proxy data (Huber and Caballero, 2011). Reconstructed SST of $14.4\pm 2.8^{\circ}\text{C}$ near the North Pole during the T-OAE, however, correspond to the maximum monthly temperatures simulated by the Turonian IPSL-CM5A2 model near the North Pole at 4x PIL (Laugié et al., 2020). The hypothesis of shell growth restricted to warmest month in the analysed Toarcian Arctic bivalves, however, remains questionable given the evidence for summertime-only growth cessation in Eocene bivalves from Antarctica (Buick and Ivany, 2004). Finally, Arctic SST as high as $15\text{-}20^{\circ}\text{C}$ are successfully achieved in the Eocene CESM1.2 CAM5 at 6 to 9x PIL (Zhu et al., 2020), in which climate sensitivity increases with rising CO_2 due to low-altitude cloud albedo feedbacks and improved radiative parameterization. As this model produces an increase in climate sensitivity with CO_2 in both Eocene and modern conditions, our results thus support the growing body of evidence that the amplitude of the future anthropogenic warming may be underestimated by conventional state-of-the-art models. The reconstruction of $\delta^{18}\text{O}_w$ values using proxy data provides a complementary aspect to assess model capabilities, as this indicator is sensitive to both climate parameters (moisture, humidity and temperatures) and

paleogeography. Our mid-latitude $\delta^{18}\text{O}_w$ are broadly similar to those reconstructed using marine turtle bones $\delta^{18}\text{O}_{\text{PO}_4}$ and Δ_{47} data from Jurassic to Eocene bivalves, ammonites, and foraminifera, as well as belemnites (Fig. 5, Billon-Bruyat et al., 2005; Coulson et al., 2011; van Baal et al., 2013; Evans et al., 2018; Wierzbowski et al., 2018; Vickers et al., 2021; de Winter et al., 2021). The reconstructed $\delta^{18}\text{O}_w$ values are, to some extent, also broadly comparable with those inferred from belemnite calcite Δ_{47} data (Wierzbowski et al., 2018; Vickers et al., 2019, 2020, 2021; Price et al., 2020), although such data should be interpreted with caution owing to the likely unique oxygen isotope fractionation of belemnite calcite (Price et al., 2020; Vickers et al., 2021). As for temperatures, regional processes in the Western Interior Seaway explains the mid-latitude very low $\delta^{18}\text{O}_w$ indicated by most late Cretaceous Δ_{47} data (Petersen et al., 2016). In line with evidence for substantial ^{18}O -depletion of Toarcian Arctic waters (relative to VSMOW) suggested by our data, previous studies suggested low $\delta^{18}\text{O}_w$ values in interior seas border by large continental areas, such in the Western Interior Seaway during the Campanian-Maastrichtian (Coulson et al., 2011; Petersen et al., 2016b; Meyer et al., 2018) and Middle Russian sea during Middle to Late Jurassic interval (Wierzbowski et al., 2018). Interestingly, the Δ_{47} temperatures reported in these basins are also differ markedly from those reported in more open-oceans sites of similar age and paleo-latitude, suggesting the possible influence of colder Arctic water masses through southward ocean currents. Indeed the Middle to Late Jurassic Δ_{47} temperatures reported in the Middle Russian sea (Wierzbowski et al., 2018) are $\sim 10^\circ\text{C}$ lower than coeval data from the Hebrides basin, Scotland (Vickers et al., 2020) and from the high mid-latitudes Falkland Plateau in the southern hemisphere (Vickers et al., 2019). Such anomalies in $\delta^{18}\text{O}_w$ values and temperatures demonstrate the importance of regional pattern such as river runoff and basin connections on the environmental parameters of restricted basin (Petersen et al., 2016b). More generally, local anomalies in $\delta^{18}\text{O}_w$ values evidenced by the new and earlier clumped isotope data highlight ability of this proxy of deciphering the influence of the temperature and $\delta^{18}\text{O}_w$ values in otherwise similar $\delta^{18}\text{O}_c$ dataset as well as the.

We are aware of only few-three Earth-system $\delta^{18}\text{O}_w$ simulations for the broad time intervals considered here (Zhou et al., 2008; Tindall et al., 2010; Zhu et al., 2020), hence limiting model-data comparisons. The higher freshwater contribution near high-latitude landmasses of the Northern Hemisphere in both/all these models produced lower $\delta^{18}\text{O}_w$ that are broadly consistent with previous and our proxy data (Fig. 5). This good agreement, however, might be partly fortuitous, as proxy data suggest SST much higher than those produced by both models (Fig. 5). As mentioned above (section 5.2), such higher-than-predicted polar warmth would have substantially increased high-latitude $\delta^{18}\text{O}_p$, so that higher runoff would be required to reproduce the magnitude of the poleward drop in $\delta^{18}\text{O}_w$ indicated by proxy data. This highlights the usefulness, in future models of past greenhouse climates, to systematically provide $\delta^{18}\text{O}_w$ predictions so that $\delta^{18}\text{O}_w$ estimates derived from Δ_{47} data may serve as a constraint on Earth system models.

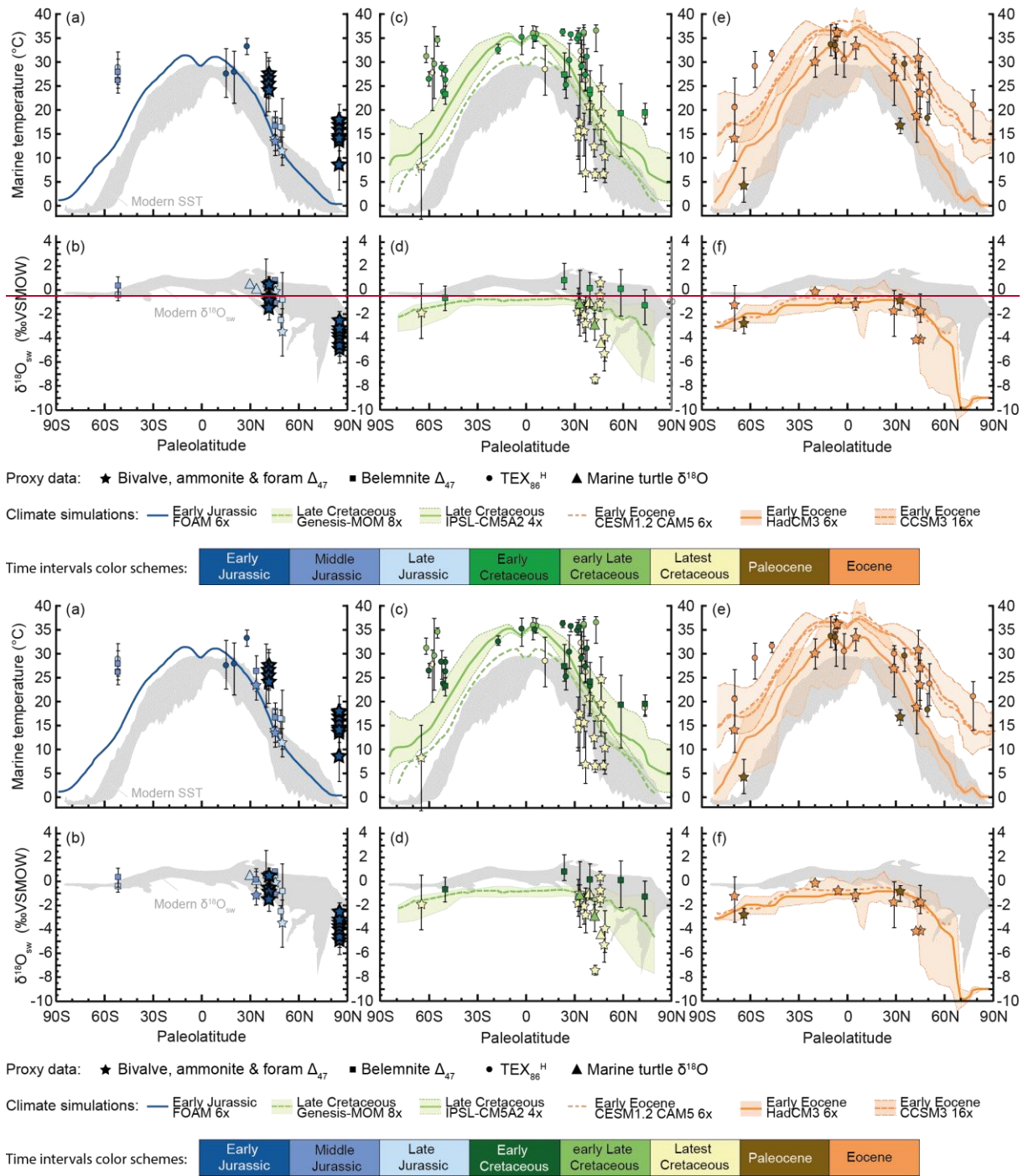


Figure 5. Comparison of the new (bold outline) reconstructed Early Jurassic SST and $\delta^{18}\text{O}_{\text{sw}}$ with published Jurassic-Eocene proxy-based reconstructions (thin outline) and Earth system simulations.

Proxy-model comparison of SST and $\delta^{18}\text{O}_{\text{sw}}$ are shown for the Jurassic (a, b), the Cretaceous (c, d) and the Early Paleogene (e, f). Proxy data are divided between 8 time slices based on their definition in the International Chronostratigraphic chart v2020/03 (Cohen et al., 2013; updated); early Late Cretaceous=Cenomanian to Santonian; Latest Cretaceous=Campanian-Maastrichtian. Marker colour in proxy data shows sample age accordingly (see key). New data are displayed as the reported value and its associated uncertainties for each samples. Datasets from the literature, from the same proxy and location, were regrouped within each time slice. The marker displays the mean of available data and the error bar the extent of the data (minimal to maximal value). Both Δ_{47} and $\text{TEX}_{86}^{\text{H}}$ temperatures are published temperatures. $\delta^{18}\text{O}_{\text{w}}$ were recomputed using published

Δ_{47} temperatures and $\delta^{18}\text{O}_c$ with the following fractionation equations: belemnite calcite: (Coplen, (2007), aragonite: (Grossman and Ku,(-1986), bivalve calcite: (Epstein et al., (1953), foraminifera: (Erez and Luz, (1983), turtle bones: (Barrick et al., (1999) updated (Pouech et al., 2014). Results of Earth system simulations are shown as annual averages (bold lines) and summer and winter seasonal averages (colour shading). Modern range of SST and $\delta^{18}\text{O}_{sw}$ are also shown (grey shading) for comparison. Δ_{47} data are from: Keating-Bitonti et al., 2011; Douglas et al., 2014; Petersen et al., 2016b, a; Evans et al., 2018; Wierzbowski et al., 2018; Meyer et al., 2018; Vickers et al., 2019, 2020, 2021; Price et al., 2020; Brigaud et al., 2020; Fernandez et al., 2021; de Winter et al., 2021. TEX_{86}^H paleothermometry data are from: Jenkyns et al., 2012; Lunt et al., 2012; Douglas et al., 2014; Frieling et al., 2014; O'Brien et al., 2017; Robinson et al., 2017; Cramwinckel et al., 2018; O'Connor et al., 2019; Ruebsam et al., 2020; Cavalheiro et al., 2021 . Marine turtle phosphate $\delta^{18}\text{O}$ data are from : Billon-Bruyat et al. (2005), Coulson et al. (2011), van Baal et al. (2013). The FOAM 6x simulation is from Dera and Donnadiou (2012), Genesis-MOM 8x simulation is from Zhou et al. (2008), IPSL-CM5A2 4x is from Laugié et al. (2020), CESMA.2 CAM5 6x is from Zhu et al. (2020), HadCM3 6x is from Tindall et al. (2010), CCSM3 16x is from Huber and Caballero (2011), with N_x indicating CO_2 levels used in the simulations as a multiple of preindustrial level (i.e. 280ppm). More detailed information on the building of this figure and the data compilation is available as Supplementary material. See supplement for references used in this compilation.

6 Conclusion

The clumped isotope compositions of pristine, minimally buried, marine molluscs shells yield SST $>25^\circ\text{C}$ at mid-latitudes during the early Pliensbachian and SST $>10^\circ\text{C}$ at polar paleolatitudes during the T-OAE. The reconstructed $\delta^{18}\text{O}_w$ values point to higher freshwater contribution toward Arctic regions, illustrating the dangers of assuming a fixed global $\delta^{18}\text{O}_w$ value for $\delta^{18}\text{O}$ -derived temperature reconstructions. Although further work should clarify the influence of seasonal changes in the recorded SST values at polar sites, these results strengthen a growing body of evidence for higher climate sensitivity under high atmospheric CO_2 conditions and suggest that this higher sensitivity is a general feature of greenhouse climates since at least 180 Ma.

Data availability

Detailed data supporting this study are available in the supplementary material. Raw data are available on request to the author.

Author contribution

TL and GS designed the study and led the writing in close cooperation with CL, MR and MD. MR and GS participated to the field work and collected the samples. TL prepared and sampled the shell material for geochemistry and performed the SEM observations. MR, JS and OL identified the fossils. MD and TL performed the clumped isotope analyses and data processing. AV-L and TL performed the stable isotopes analyses and data processing. BR, GM and TL gathered and interpreted the Raman spectra. TL and GS compiled the paleotemperature proxy database. All authors were involved in the interpretation of the results.

Competing interest

The authors declare that they have no conflict of interest.

Acknowledgments

This research was funded by the ANR OXYMORE (ANR-18-CE31-0020), [joint CNRS/RFBF International Emerging Action grant 205700](#) and RFBF grant 21-55-15015. [JS was supported by grant APVV 17-0555](#). We thank Ghislaine Broillet for her help with SEM analyses, and Ophélie Lodyga for help with Raman analyses. [We thank two anonymous reviewers for their constructive suggestions and comments that substantially improved the manuscript.](#)

References

Anderson, N. T., Kelson, J. R., Kele, S., Daëron, M., Bonifacie, M., Horita, J., Mackey, T. J., John, C. M., Kluge, T., Petschnig, P., Jost, A. B., Huntington, K. W., Bernasconi, S. M., and Bergmann, K. D.: A unified clumped isotope thermometer calibration (0.5–1100°C) using carbonate-based standardization, *Geophys Res Lett*, <https://doi.org/10.1029/2020GL092069>, 2021.

van Baal, R. R., Janssen, R., van der Lubbe, H. J. L., Schulp, A. S., Jagt, J. W. M., and Vonhof, H. B.: Oxygen and carbon stable isotope records of marine vertebrates from the type Maastrichtian, The Netherlands and northeast Belgium (Late Cretaceous), *Palaeogeography, Palaeoclimatology, Palaeoecology*, 392, 71–78, <https://doi.org/10.1016/j.palaeo.2013.08.020>, 2013.

Baghli, H., Mattioli, E., Spangenberg, J. E., Bensalah, M., Arnaud-Godet, F., Pittet, B., and Suan, G.: Early Jurassic climatic trends in the south-Tethyan margin, *Gondwana Research*, 77, 67–81, 2020.

Barrick, R. E., Fischer, A. G., and Showers, W. J.: Oxygen isotopes from turtle bone; applications for terrestrial paleoclimates?, *PALAIOS*, 14, 186–191, <https://doi.org/10.2307/3515374>, 1999.

Bernasconi, S. M., Müller, I. A., Bergmann, K. D., Breitenbach, S. F. M., Fernandez, A., Hodell, D. A., Jaggi, M., Meckler, A. N., Millan, I., and Ziegler, M.: Reducing Uncertainties in Carbonate Clumped Isotope Analysis Through Consistent Carbonate-Based Standardization, *Geochem Geophys Geosyst*, 19, 2895–2914, <https://doi.org/10.1029/2017GC007385>, 2018.

Bernasconi, S. M., Daëron, M., Bergmann, K. D., Bonifacie, M., Meckler, A. N., Affek, H. P., Anderson, N., Bajnai, D., Barkan, E., Beverly, E., Blamart, D., Burgener, L., Calmels, D., Chaduteau, C., Clog, M., Davidheiser-Kroll, B., Davies, A., Dux, F., Eiler, J., Elliott, B., Fetrow, A. C., Fiebig, J., Goldberg, S., Hermoso, M., Huntington, K. W., Hyland, E., Ingalls, M., Jaggi, M., John, C. M., Jost, A. B., Katz, S., Kelson, J., Kluge, T., Kocken, I. J., Laskar, A., Leutert, T. J., Liang, D., Lucarelli, J., Mackey, T. J., Manganot, X., Meinicke, N., Modestou, S. E., Müller, I. A., Murray, S., Neary, A., Packard, N., Passey, B. H., Pelletier, E., Petersen, S., Piasecki, A., Schauer, A., Snell, K. E., Swart, P. K., Tripathi, A., Upadhyay, D., Vennemann, T., Winkelstern, I., Yarian, D., Yoshida, N., Zhang, N., and Ziegler, M.: InterCarb: A Community Effort to Improve Interlaboratory Standardization of the Carbonate Clumped Isotope Thermometer Using Carbonate Standards, *Geochem Geophys Geosyst*, 22, <https://doi.org/10.1029/2020GC009588>, 2021.

Billon-Bruyat, J.-P., Lécuyer, C., Martineau, F., and Mazin, J.-M.: Oxygen isotope compositions of Late Jurassic vertebrate remains from lithographic limestones of western Europe: implications for the ecology of fish, turtles, and crocodylians, *Palaeogeography, Palaeoclimatology, Palaeoecology*, 216, 359–375, <https://doi.org/10.1016/j.palaeo.2004.11.011>, 2005.

Blaise, T., Barbarand, J., Kars, M., Ploquin, F., Aubourg, C., Brigaud, B., Cathelineau, M., El Albani, A., Gautheron, C., Izart, A., Janots, D., Michels, R., Pagel, M., Pozzi, J.-P., Boiron, M.-C., and Landrein, P.: Reconstruction of low temperature (<100 °C) burial in sedimentary basins: A comparison of geothermometer in the intracontinental Paris Basin, *Marine and Petroleum Geology*, 53, 71–87, <https://doi.org/10.1016/j.marpetgeo.2013.08.019>, 2014.

- 550 Bougeault, C., Pellenard, P., Deconinck, J.-F., Hesselbo, S. P., Dommergues, J.-L., Bruneau, L., Cocquerez, T., Laffont, R., Huret, E., and Thibault, N.: Climatic and palaeoceanographic changes during the Pliensbachian (Early Jurassic) inferred from clay mineralogy and stable isotope (C-O) geochemistry (NW Europe), *Global and Planetary Change*, 149, 139–152, <https://doi.org/10.1016/j.gloplacha.2017.01.005>, 2017.
- Brigaud, B., Bonifacie, M., Pagel, M., Blaise, T., Calmels, D., Haurine, F., and Landrein, P.: Past hot fluid flows in limestones detected by $\Delta 47$ -(U-Pb) and not recorded by other geothermometers, *Geology*, 48, 851–856, <https://doi.org/10.1130/G47358.1>, 2020.
- 555 Buick, D. P. and Ivany, L. C.: 100 years in the dark: Extreme longevity of Eocene bivalves from Antarctica, *Geology*, 32, 921–924, <https://doi.org/10.1130/G20796.1>, 2004.
- Cavalheiro, L., Wagner, T., Steinig, S., Bottini, C., Dummann, W., Esegbue, O., Gambacorta, G., Giraldo-Gómez, V., Farnsworth, A., Flögel, S., Hofmann, P., Lunt, D. J., Rethemeyer, J., Torricelli, S., and Erba, E.: Impact of global cooling on Early Cretaceous high pCO₂ world during the Weissert Event, *Nat Commun*, 12, 5411, <https://doi.org/10.1038/s41467-021-25706-0>, 2021.
- 560 Chen, S., Ryb, U., Piasecki, A. M., Lloyd, M. K., Baker, M. B., and Eiler, J. M.: Mechanism of solid-state clumped isotope reordering in carbonate minerals from aragonite heating experiments, *Geochimica et Cosmochimica Acta*, 258, 156–173, <https://doi.org/10.1016/j.gca.2019.05.018>, 2019.
- Cohen, K. M., Finney, S. C., Gibbard, P. L., and Fan, J.-X.: The ICS International Chronostratigraphic Chart, 36, 199–204, 2013.
- 565 Coplen, T. B.: Calibration of the calcite–water oxygen-isotope geothermometer at Devils Hole, Nevada, a natural laboratory, *Geochimica et Cosmochimica Acta*, 71, 3948–3957, <https://doi.org/10.1016/j.gca.2007.05.028>, 2007.
- Coulson, A. B., Kohn, M. J., and Barrick, R. E.: Isotopic evaluation of ocean circulation in the Late Cretaceous North American seaway, *Nature Geosci*, 4, 852–855, <https://doi.org/10.1038/ngeo1312>, 2011.
- 570 Craig, N.: Growth of the bivalve *Nucula annulata* in nutrient-enriched environments, *Mar. Ecol. Prog. Ser.*, 104, 77–90, <https://doi.org/10.3354/meps104077>, 1994.
- Cramwinckel, M. J., Huber, M., Kocken, I. J., Agnini, C., Bijl, P. K., Bohaty, S. M., Frieling, J., Goldner, A., Hilgen, F. J., Kip, E. L., Peterse, F., van der Ploeg, R., Röhl, U., Schouten, S., and Sluijs, A.: Synchronous tropical and polar temperature evolution in the Eocene, *Nature*, 559, 382–386, <https://doi.org/10.1038/s41586-018-0272-2>, 2018.
- 575 Daëron, M.: Full Propagation of Analytical Uncertainties in $\Delta 47$ Measurements, *Geochem. Geophys. Geosyst.*, 22, <https://doi.org/10.1029/2020GC009592>, 2021.
- 580 Daëron, M., Blamart, D., Peral, M., and Affek, H. P.: Absolute isotopic abundance ratios and the accuracy of $\Delta 47$ measurements, *Chemical Geology*, 442, 83–96, <https://doi.org/10.1016/j.chemgeo.2016.08.014>, 2016.
- Dera, G. and Donnadieu, Y.: Modeling evidences for global warming, Arctic seawater freshening, and sluggish oceanic circulation during the Early Toarcian anoxic event, *Paleoceanography*, 27, <https://doi.org/10.1029/2012PA002283>, 2012.
- 585 Dera, G., Pucéat, E., Pellenard, P., Neige, P., Delsate, D., Joachimski, M. M., Reisberg, L., and Martinez, M.: Water mass exchange and variations in seawater temperature in the NW Tethys during the Early Jurassic: Evidence from neodymium and oxygen isotopes of fish teeth and belemnites, *Earth and Planetary Science Letters*, 286, 198–207, <https://doi.org/10.1016/j.epsl.2009.06.027>, 2009.

- 590 Dera, G., Brigaud, B., Monna, F., Laffont, R., Pucéat, E., Deconinck, J.-F., Pellenard, P., Joachimski, M. M., and Durllet, C.: Climatic ups and downs in a disturbed Jurassic world, *Geology*, 39, 215–218, 2011.
- van Dijk, J., Fernandez, A., Bernasconi, S. M., Caves Rugenstein, J. K., Passey, S. R., and White, T.: Spatial pattern of super-greenhouse warmth controlled by elevated specific humidity, *Nature Geoscience*, 13, 739–744, <https://doi.org/10.1038/s41561-020-00648-2>, 2020.
- 595 Disnar, J. R., Le Strat, P., Farjanel, G., and Fikri, A.: Sédimentation de la matière organique dans le nord-est du Bassin de Paris: conséquences sur le dépôt des argilites carbonées du Toarcien inférieur (Organic matter sedimentation in the northeast of the Paris Basin: consequences on the deposition of the lower toarcian black shales), *Chemical Geology*, 131, 15–35, [https://doi.org/10.1016/0009-2541\(96\)00021-6](https://doi.org/10.1016/0009-2541(96)00021-6), 1996.
- 600 Douglas, P. M. J., Affek, H. P., Ivany, L. C., Houben, A. J. P., Sijp, W. P., Sluijs, A., Schouten, S., and Pagani, M.: Pronounced zonal heterogeneity in Eocene southern high-latitude sea surface temperatures, *Proceedings of the National Academy of Sciences*, 111, 6582–6587, <https://doi.org/10.1073/pnas.1321441111>, 2014.
- 605 Epstein, S., Buchsbaum, R., Lowenstam, H. A., and Urey, H. C.: Revised carbonate-water isotopic temperature scale, *Geol Soc America Bull*, 64, 1315, [https://doi.org/10.1130/0016-7606\(1953\)64\[1315:RCITS\]2.0.CO;2](https://doi.org/10.1130/0016-7606(1953)64[1315:RCITS]2.0.CO;2), 1953.
- Erez, J. and Luz, B.: Experimental paleotemperature equation for planktonic foraminifera, *Geochimica et Cosmochimica Acta*, 47, 1025–1031, 1983.
- 610 Evans, D., Sagoo, N., Renema, W., Cotton, L. J., Müller, W., Todd, J. A., Saraswati, P. K., Stassen, P., Ziegler, M., Pearson, P. N., Valdes, P. J., and Affek, H. P.: Eocene greenhouse climate revealed by coupled clumped isotope-Mg/Ca thermometry, *Proc Natl Acad Sci USA*, 115, 1174–1179, <https://doi.org/10.1073/pnas.1714744115>, 2018.
- 615 Fernandez, A., Korte, C., Ullmann, C. V., Looser, N., Wohlwend, S., and Bernasconi, S. M.: Reconstructing the magnitude of Early Toarcian (Jurassic) warming using the reordered clumped isotope compositions of belemnites, *Geochimica et Cosmochimica Acta*, 293, 308–327, <https://doi.org/10.1016/j.gca.2020.10.005>, 2021.
- Frieling, J., Iakovleva, A. I., Reichart, G.-J., Aleksandrova, G. N., Gnibidenko, Z. N., Schouten, S., and Sluijs, A.: Paleocene–Eocene warming and biotic response in the epicontinental West Siberian Sea, *Geology*, 42, 767–770, <https://doi.org/10.1130/G35724.1>, 2014.
- 620 Grossman, E. L. and Ku, T.-L.: Oxygen and carbon isotope fractionation in biogenic aragonite: temperature effects, *Chemical Geology*, 59, 59–74, [https://doi.org/10.1016/0168-9622\(86\)90057-6](https://doi.org/10.1016/0168-9622(86)90057-6), 1986.
- 625 Hemingway, J. D. and Henkes, G. A.: A disordered kinetic model for clumped isotope bond reordering in carbonates, *Earth and Planetary Science Letters*, 566, 116962, <https://doi.org/10.1016/j.epsl.2021.116962>, 2021.
- Henkes, G. A., Passey, B. H., Grossman, E. L., Shenton, B. J., Pérez-Huerta, A., and Yancey, T. E.: Temperature limits for preservation of primary calcite clumped isotope paleotemperatures, *Geochimica et Cosmochimica Acta*, 139, 362–382, <https://doi.org/10.1016/j.gca.2014.04.040>, 2014.
- 630 van Hinsbergen, D. J. J., de Groot, L. V., van Schaik, S. J., Spakman, W., Bijl, P. K., Sluijs, A., Langereis, C. G., and Brinkhuis, H.: A Paleolatitude Calculator for Paleoclimate Studies, *PLOS ONE*, 10, e0126946, <https://doi.org/10.1371/journal.pone.0126946>, 2015.

- Huber, M. and Caballero, R.: The Early Eocene Equable Climate Problem Revisited, *Clim. Past*, 7, 603–633, <https://doi.org/10.5194/cp-7-603-2011>, 2011.
- 635 Jenkyns, H. C. and Clayton, C. J.: Black shales and carbon isotopes in pelagic sediments from the Tethyan Lower Jurassic, *Sedimentology*, 33, 87–106, <https://doi.org/10.1111/j.1365-3091.1986.tb00746.x>, 1986.
- Jenkyns, H. C., Schouten-Huibers, L., Schouten, S., and Sinninghe Damsté, J. S.: Warm Middle Jurassic–Early Cretaceous high-latitude sea-surface temperatures from the Southern Ocean, *Clim. Past*, 8, 215–226, <https://doi.org/10.5194/cp-8-215-2012>, 2012.
- 640 Keating-Bitonti, C. R., Ivany, L. C., Affek, H. P., Douglas, P., and Samson, S. D.: Warm, not super-hot, temperatures in the early Eocene subtropics, *Geology*, 39, 771–774, <https://doi.org/10.1130/G32054.1>, 2011.
- Kerimov, V. Yu., Shcherbina, Yu. V., and Ivanov, A. A.: Formation conditions and evolution of oil and gas source strata of the Laptev sea shelf ore and gas province, *Izvestiya Vysshikh Uchebnykh Zavedeniy. Geologiya i Razvedka*, 46–59, <https://doi.org/10.32454/0016-7762-2020-63-3-46-59>, 2020.
- 645 Killam, D. E. and Clapham, M. E.: Identifying the ticks of bivalve shell clocks: seasonal growth in relation to temperature and food supply, *PALAIOS*, 33, 228–236, <https://doi.org/10.2110/palo.2017.072>, 2018.
- 650 Kim, S.-T. and O’Neil, J. R.: Equilibrium and nonequilibrium oxygen isotope effects in synthetic carbonates, *Geochimica et Cosmochimica Acta*, 61, 3461–3475, [https://doi.org/10.1016/S0016-7037\(97\)00169-5](https://doi.org/10.1016/S0016-7037(97)00169-5), 1997.
- Kim, S.-T., Mucci, A., and Taylor, B. E.: Phosphoric acid fractionation factors for calcite and aragonite between 25 and 75 °C: Revisited, *Chemical Geology*, 246, 135–146, <https://doi.org/10.1016/j.chemgeo.2007.08.005>, 2007.
- 655 Krencker, F. N., Bodin, S., Hoffmann, R., Suan, G., Mattioli, E., Kabiri, L., Föllmi, K. B., and Immenhauser, A.: The middle Toarcian cold snap: Trigger of mass extinction and carbonate factory demise, *Global and Planetary Change*, 15, 2014.
- 660 Laugié, M., Donnadieu, Y., Ladant, J.-B., Green, J. A. M., Bopp, L., and Raison, F.: Stripping back the modern to reveal the Cenomanian–Turonian climate and temperature gradient underneath, *Clim. Past*, 16, 953–971, <https://doi.org/10.5194/cp-16-953-2020>, 2020.
- Li, X., Wang, J., Rasbury, T., Zhou, M., Wei, Z., and Zhang, C.: Early Jurassic climate and atmospheric CO₂ concentration in the Sichuan paleobasin, southwestern China, 16, 2055–2074, <https://doi.org/10.5194/cp-16-2055-2020>, 2020.
- 665 Lunt, D. J., Dunkley Jones, T., Heinemann, M., Huber, M., LeGrande, A., Winguth, A., Loftson, C., Marotzke, J., Roberts, C. D., Tindall, J., Valdes, P., and Winguth, C.: A model–data comparison for a multi-model ensemble of early Eocene atmosphere–ocean simulations: EoMIP, *Clim. Past*, 8, 1717–1736, <https://doi.org/10.5194/cp-8-1717-2012>, 2012.
- 670 Markwick, P. J.: Fossil crocodylians as indicators of Late Cretaceous and Cenozoic climates: implications for using palaeontological data in reconstructing palaeoclimate, *Palaeogeography, Palaeoclimatology, Palaeoecology*, 137, 205–271, [https://doi.org/10.1016/S0031-0182\(97\)00108-9](https://doi.org/10.1016/S0031-0182(97)00108-9), 1998.

- 675 McElwain, J. C., Wade-Murphy, J., and Hesselbo, S. P.: Changes in carbon dioxide during an oceanic anoxic event linked to intrusion into Gondwana coals, *Nature*, 435, 479–482, <https://doi.org/10.1038/nature03618>, 2005.
- Meyer, K. W., Petersen, S. V., Lohmann, K. C., and Winkelstern, I. Z.: Climate of the Late Cretaceous North American Gulf and Atlantic Coasts, *Cretaceous Research*, 89, 160–173, <https://doi.org/10.1016/j.cretres.2018.03.017>, 2018.
- 680 Nikitenko, B. L. and Mickey, M. B.: Foraminifera and ostracodes across the Pliensbachian-Toarcian boundary in the Arctic Realm (stratigraphy, palaeobiogeography and biofacies), Geological Society, London, Special Publications, 230, 137–174, <https://doi.org/10.1144/GSL.SP.2004.230.01.08>, 2004.
- 685 Nikitenko, B. L., Shurygin, B. N., Knyazev, V. G., Meledina, S. V., Dzyuba, O. S., Lebedeva, N. K., Peshchevitskaya, E. B., Glinskikh, L. A., Goryacheva, A. A., and Khafaeva, S. N.: Jurassic and Cretaceous stratigraphy of the Anabar area (Arctic Siberia, Laptev Sea coast) and the Boreal zonal standard, *Russian Geology and Geophysics*, 54, 808–837, <https://doi.org/10.1016/j.rgg.2013.07.005>, 2013.
- 690 Nooitgedacht, C. W., van der Lubbe, H. J. L., Ziegler, M., and Staudigel, P. T.: Internal water facilitates thermal resetting of clumped isotopes in biogenic aragonite, *Geochem Geophys Geosyst*, <https://doi.org/10.1029/2021GC009730>, 2021.
- 695 O'Brien, C. L., Robinson, S. A., Pancost, R. D., Sinninghe Damsté, J. S., Schouten, S., Lunt, D. J., Alsenz, H., Bornemann, A., Bottini, C., Brassell, S. C., Farnsworth, A., Forster, A., Huber, B. T., Inglis, G. N., Jenkyns, H. C., Linnert, C., Littler, K., Markwick, P., McAnena, A., Mutterlose, J., Naafs, B. D. A., Püttmann, W., Sluijs, A., van Helmond, N. A. G. M., Vellekoop, J., Wagner, T., and Wrobel, N. E.: Cretaceous sea-surface temperature evolution: Constraints from TEX 86 and planktonic foraminiferal oxygen isotopes, *Earth-Science Reviews*, 172, 224–247, <https://doi.org/10.1016/j.earscirev.2017.07.012>, 2017.
- 700 O'Connor, L. K., Robinson, S. A., Naafs, B. D. A., Jenkyns, H. C., Henson, S., Clarke, M., and Pancost, R. D.: Late Cretaceous Temperature Evolution of the Southern High Latitudes: A TEX86 Perspective, *Paleoceanography and Paleoclimatology*, 19, 2019.
- Pagani, M., Pedentchouk, N., Huber, M., Sluijs, A., Schouten, S., Brinkhuis, H., Damste, J. S. S., and Dickens, G. R.: Arctic hydrology during global warming at the Palaeocene/Eocene thermal maximum, *Nature*, 442, 671–675, <https://doi.org/10.1038/nature05043>, 2006.
- 705 Peck, L. S., Colman, J. G., and Murray, A. W. A.: Growth and tissue mass cycles in the infaunal bivalve *Yoldia eightsi* at Signy Island, Antarctica, *Polar Biology*, 23, 420–428, <https://doi.org/10.1007/s003000050463>, 2000.
- Petersen, S. V., Dutton, A., and Lohmann, K. C.: End-Cretaceous extinction in Antarctica linked to both Deccan volcanism and meteorite impact via climate change, *Nat Commun*, 7, 12079, <https://doi.org/10.1038/ncomms12079>, 2016a.
- 710 Petersen, S. V., Tabor, C. R., Lohmann, K. C., Poulsen, C. J., Meyer, K. W., Carpenter, S. J., Erickson, J. M., Matsunaga, K. K. S., Smith, S. Y., and Sheldon, N. D.: Temperature and salinity of the Late Cretaceous Western Interior Seaway, *Geology*, 44, 903–906, <https://doi.org/10.1130/G38311.1>, 2016b.
- 715 Pouech, J., Amiot, R., Lécuyer, C., Mazin, J.-M., Martineau, F., and Fourrel, F.: Oxygen isotope composition of vertebrate phosphates from Cherves-de-Cognac (Berriasian, France): Environmental and ecological significance, *Palaeogeography, Palaeoclimatology, Palaeoecology*, 410, 290–299, <https://doi.org/10.1016/j.palaeo.2014.05.036>, 2014.

- 720 Price, G. D., Bajnai, D., and Fiebig, J.: Carbonate clumped isotope evidence for latitudinal seawater temperature gradients and the oxygen isotope composition of Early Cretaceous seas, *Palaeogeography, Palaeoclimatology, Palaeoecology*, 552, 109777, <https://doi.org/10.1016/j.palaeo.2020.109777>, 2020.
- Robinson, S. A., Ruhl, M., Astley, D. L., Naafs, B. D. A., Farnsworth, A. J., Bown, P. R., Jenkyns, H. C., Lunt, D. J., O'Brien, C., Pancost, R. D., and Markwick, P. J.: Early Jurassic North Atlantic sea-surface temperatures from TEX₈₆ palaeothermometry, *Sedimentology*, 64, 215–230, <https://doi.org/10.1111/sed.12321>, 2017.
- 725 Roche, D. M., Donnadieu, Y., Pucéat, E., and Paillard, D.: Effect of changes in $\delta^{18}\text{O}$ content of the surface ocean on estimated sea surface temperatures in past warm climate, *Paleoceanography*, 21, n/a–n/a, <https://doi.org/10.1029/2005PA001220>, 2006.
- Rogov, M. A., Zverkov, N. G., Zakharov, V. A., and Arkhangelsky, M. S.: Marine Reptiles and Climates of the Jurassic and Cretaceous of Siberia, *Stratigr. Geol. Correl.*, 27, 398–423, <https://doi.org/10.1134/S0869593819040051>, 2019.
- 730 Rozanski, K., Araguas-Araguas, L., and Gonfiantini, R.: Relation Between Long-Term Trends of Oxygen-18 Isotope Composition of Precipitation and Climate, *Science*, 258, 981–985, <https://doi.org/10.1126/science.258.5084.981>, 1992.
- 735 Ruebsam, W., Reolid, M., Sabatino, N., Masetti, D., and Schwark, L.: Molecular paleothermometry of the early Toarcian climate perturbation, *Global and Planetary Change*, 195, 103351, <https://doi.org/10.1016/j.gloplacha.2020.103351>, 2020.
- Schöne, B. R.: The curse of physiology—challenges and opportunities in the interpretation of geochemical data from mollusk shells, *Geo-Mar Lett*, 28, 269–285, <https://doi.org/10.1007/s00367-008-0114-6>, 2008.
- 740 Shackleton, N. J. and Kennett, J. P.: Paleotemperature history of the Cenozoic and the initiation of Antarctic glaciation: oxygen and carbon isotope analyses in DSDP Sites 277, 279, and 281, *Initial Reports of Deep Sea Drilling*, 29, 743–756, 1975.
- 745 Sluijs, A., Schouten, S., Pagani, M., Woltering, M., Brinkhuis, H., Damsté, J. S. S., Dickens, G. R., Huber, M., Reichert, G.-J., Stein, R., Matthiessen, J., Lourens, L. J., Pedentchouk, N., Backman, J., Moran, K., and the Expedition 302 Scientists: Subtropical Arctic Ocean temperatures during the Palaeocene/Eocene thermal maximum, *Nature*, 441, 610–613, <https://doi.org/10.1038/nature04668>, 2006.
- 750 Sluijs, A., Frieling, J., Inglis, G. N., Nierop, K. G. J., Peterse, F., Sangiorgi, F., and Schouten, S.: Late Paleocene – early Eocene Arctic Ocean Sea Surface Temperatures; reassessing biomarker paleothermometry at Lomonosov Ridge, *Proxy Use-Development-Validation/Marine Archives/Cenozoic*, <https://doi.org/10.5194/cp-2020-13>, 2020.
- Stolper, D. A. and Eiler, J. M.: The kinetics of solid-state isotope-exchange reactions for clumped isotopes: A study of inorganic calcites and apatites from natural and experimental samples, *American Journal of Science*, 315, 363–411, <https://doi.org/10.2475/05.2015.01>, 2015.
- 755 Suan, G., Mattioli, E., Pittet, B., Lécuyer, C., Suchéras-Marx, B., Duarte, L. V., Philippe, M., Reggiani, L., and Martineau, F.: Secular environmental precursors to Early Toarcian (Jurassic) extreme climate changes, *Earth and Planetary Science Letters*, 11, 2010.
- Suan, G., Nikitenko, B. L., Rogov, M. A., Baudin, F., Spangenberg, J. E., Knyazev, V. G., Glinskikh, L. A., Goryacheva, A. A., Adatte, T., Riding, J. B., Föllmi, K. B., Pittet, B., Mattioli, E., and Lécuyer,

- 760 C.: Polar record of Early Jurassic massive carbon injection, *Earth and Planetary Science Letters*, 312, 102–113, <https://doi.org/10.1016/j.epsl.2011.09.050>, 2011.
- Suan, G., Popescu, S.-M., Suc, J.-P., Schnyder, J., Fauquette, S., Baudin, F., Yoon, D., Piepjohn, K., Sobolev, N. N., and Labrousse, L.: Subtropical climate conditions and mangrove growth in Arctic Siberia during the early Eocene, *Geology*, 45, 539–542, <https://doi.org/10.1130/G38547.1>, 2017.
- 765 Thierry, J.: Middle Toarcian map. 8, in: Dercourt, J., Gaetani, M., Vrielynck, B., Barrier, E., Biju-Duval, B., Brunet, M.F. ... Sandulescu, M. (Eds.), *Atlas Peri-Tethys Palaeogeographical Maps.*, CCGM/CGMW, Paris, 61–70, 2000.
- Thuy, B., Gale, A. S., and Reich, M.: A new echinoderm Lagerstätte from the Pliensbachian (Early Jurassic) of the French Ardennes, *Swiss J Palaeontol*, 130, 173–185, <https://doi.org/10.1007/s13358-010-0015-y>, 2011.
- 770 Tindall, J., Flecker, R., Valdes, P., Schmidt, D. N., Markwick, P., and Harris, J.: Modelling the oxygen isotope distribution of ancient seawater using a coupled ocean–atmosphere GCM: Implications for reconstructing early Eocene climate, *Earth and Planetary Science Letters*, 292, 265–273, <https://doi.org/10.1016/j.epsl.2009.12.049>, 2010.
- 775 Torsvik, T. H., Van der Voo, R., Preeden, U., Mac Niocaill, C., Steinberger, B., Doubrovine, P. V., van Hinsbergen, D. J. J., Domeier, M., Gaina, C., Tohver, E., Meert, J. G., McCausland, P. J. A., and Cocks, L. R. M.: Phanerozoic polar wander, palaeogeography and dynamics, *Earth-Science Reviews*, 114, 325–368, <https://doi.org/10.1016/j.earscirev.2012.06.007>, 2012.
- Ullmann, C. V., Boyle, R., Duarte, L. V., Hesselbo, S. P., Kasemann, S. A., Klein, T., Lenton, T. M., Piazza, V., and Aberhan, M.: Warm afterglow from the Toarcian Oceanic Anoxic Event drives the success of deep-adapted brachiopods, *Sci Rep*, 10, 6549, <https://doi.org/10.1038/s41598-020-63487-6>, 2020.
- 780 Vickers, M. L., Bajnai, D., Price, G. D., Linckens, J., and Fiebig, J.: Southern high-latitude warmth during the Jurassic–Cretaceous: New evidence from clumped isotope thermometry, *Geology*, 47, 724–728, <https://doi.org/10.1130/G46263.1>, 2019.
- 785 Vickers, M. L., Fernandez, A., Hesselbo, S. P., Price, G. D., Bernasconi, S. M., Lode, S., Ullmann, C. V., Thibault, N., Hougard, I. W., and Korte, C.: Unravelling Middle to Late Jurassic palaeoceanographic and palaeoclimatic signals in the Hebrides Basin using belemnite clumped isotope thermometry, *Earth and Planetary Science Letters*, 546, 116401, <https://doi.org/10.1016/j.epsl.2020.116401>, 2020.
- 790 Vickers, M. L., Bernasconi, S. M., Ullmann, C. V., Lode, S., Looser, N., Morales, L. G., Price, G. D., Wilby, P. R., Hougård, I. W., Hesselbo, S. P., and Korte, C.: Marine temperatures underestimated for past greenhouse climate, *Sci Rep*, 11, 19109, <https://doi.org/10.1038/s41598-021-98528-1>, 2021.
- Vihtakari, M., Renaud, P. E., Clarke, L. J., Whitehouse, M. J., Hop, H., Carroll, M. L., and Ambrose, W. G.: Decoding the oxygen isotope signal for seasonal growth patterns in Arctic bivalves, *Palaeogeography, Palaeoclimatology, Palaeoecology*, 446, 263–283, <https://doi.org/10.1016/j.palaeo.2016.01.008>, 2016.
- 795 Waterlot, G., Bonte, A., and Destombes, J.-P.: *Carte géologique de la France à 1:50 000*. [68], Renwez, France, 1960.
- 800 Wierzbowski, H., Bajnai, D., Wacker, U., Rogov, M. A., Fiebig, J., and Tesakova, E. M.: Clumped isotope record of salinity variations in the Subboreal Province at the Middle–Late Jurassic transition, *Global and Planetary Change*, 167, 172–189, <https://doi.org/10.1016/j.gloplacha.2018.05.014>, 2018.

- 805 de Winter, N. J., Müller, I. A., Kocken, I. J., Thibault, N., Ullmann, C. V., Farnsworth, A., Lunt, D. J., Claeys, P., and Ziegler, M.: Absolute seasonal temperature estimates from clumped isotopes in bivalve shells suggest warm and variable greenhouse climate, *Commun Earth Environ*, 2, 121, <https://doi.org/10.1038/s43247-021-00193-9>, 2021.
- Zakharov, V. A. and Shurygin, B. N.: Biogeography, facies and stratigraphy of the Middle Jurassic of Soviet Arctic (by bivalve molluscs), *Transactions of the Institute of Geology and Geophysics, Siberian Branch of the Academy of Science of USSR*, 352, 1–206, 1978.
- 810 Zardus, J. D.: Protobranch bivalves, in: *Advances in Marine Biology*, vol. 42, Elsevier, 1–65, [https://doi.org/10.1016/S0065-2881\(02\)42012-3](https://doi.org/10.1016/S0065-2881(02)42012-3), 2002.
- Zhou, J., Poulsen, C. J., Pollard, D., and White, T. S.: Simulation of modern and middle Cretaceous marine $\delta^{18}\text{O}$ with an ocean-atmosphere general circulation model: Modern, mid-Cretaceous seawater $\delta^{18}\text{O}$, *Paleoceanography*, 23, n/a-n/a, <https://doi.org/10.1029/2008PA001596>, 2008.
- 815 Zhu, J., Poulsen, C. J., Otto-Bliesner, B. L., Liu, Z., Brady, E. C., and Noone, D. C.: Simulation of early Eocene water isotopes using an Earth system model and its implication for past climate reconstruction, *Earth and Planetary Science Letters*, 537, 116164, <https://doi.org/10.1016/j.epsl.2020.116164>, 2020.
- 820